

# Plasmonic Properties of Concentric Nanoshells

Corey Radloff<sup>†,§</sup> and Naomi J. Halas<sup>\*,†,‡</sup>

*Department of Chemistry, and Department of Electrical and Computer Engineering,  
Rice University, Houston, Texas 77005*

*Received March 12, 2004*

## ABSTRACT

The plasmonic properties of a concentric nanoshell, or “nanomatrushka”, are investigated. The plasmon resonant modes are analyzed in terms of the plasmon hybridization model, where new resonances occur due to a hybridization of the plasmon modes of the inner metallic shell with those of the outer metallic shell. The plasmon resonant spectra of experimentally realized concentric nanoshells are analyzed in terms of dipolar and higher order multipolar hybridized plasmon modes. A size-dependent asymmetry in the splitting of the hybridized plasmon states is observed, which is related to phase retardation effects due to the nanostructure’s finite size.

The experimental development of metal-based nanoparticles and nanostructures is currently of considerable interest. This is primarily due to the usefulness of the plasmon-derived optical response of metals, which for nanostructures is a sensitive function of both geometry and material composition. Recently, the development of various metal nanoparticle morphologies has expanded the use of plasmonic nanoparticles to include a broad range of spectroscopic,<sup>1–3</sup> biomedical,<sup>4,5</sup> and photonic applications.<sup>6</sup> Various nanoparticle morphologies, such as rods,<sup>7,8</sup> shells,<sup>9,10</sup> cups,<sup>11,12</sup> rings,<sup>1,13</sup> and triangles<sup>2,4</sup> have emerged from many different synthetic procedures. This diversity of nanoparticles is complemented by a plethora of nanopatterned planar metal structures, often supporting propagating surface plasmon waves as well as localized plasmons, developed from traditional and nontraditional planar fabrication techniques.<sup>1,6,14,15</sup> Metal-based nanoparticles and nanostructures are finding useful applications in areas such as surface plasmon resonance (SPR) sensing,<sup>4,16</sup> selective enhancement of molecular spectroscopies such as the Raman effect,<sup>2,3,17</sup> and nanoscale optical waveguides.<sup>18</sup> Both the isolated response of constituent nanostructures, as well as their strong interparticle interactions and collective electrodynamic response, have been exploited in the realization of these nanostructure-based applications of plasmonics.

Early theoretical work analyzing the plasmon response of metal nanoparticles focused on the solution of Maxwell’s equations for a plane wave incident on a nanoparticle of highly symmetric geometry.<sup>19,20</sup> Subsequent theoretical ad-

vances have led to the development of computational techniques for the calculation of the electromagnetic response.<sup>21–24</sup> Quite recently, a new conceptual approach for understanding the plasmon response of metallic nanostructures, known as “plasmon hybridization”, has been developed.<sup>25</sup> In a rigorous isomorphism with molecular orbital theory, it was shown that the plasmon resonances of complex shaped nanostructures arise due to the mixing and hybridization of fixed-frequency plasmon resonances of more elementary nanostructures. An ab initio approach to the calculation of the electronic properties of metallic nanostructures yields the plasmon response in quantitative agreement with electromagnetic properties calculated using Mie scattering theory.<sup>26</sup>

The plasmon hybridization model has been used to explain the properties of nanoshells, a tunable plasmonic nanoparticle consisting of a dielectric (silica) core and a metallic (Au or Ag) shell, whose plasmon resonance is a sensitive function of the inner and outer radius of the shell layer. For this nanostructure the tunable resonances arise from the interaction and mixing of two fixed-frequency plasmons, that of a sphere (the outer surface of the metallic shell layer) and a cavity (the inner surface of the shell layer). The hybridization of the sphere and cavity plasmons gives rise to two new plasmon oscillation modes, referred to as “bonding” and “antibonding” plasmons in analogy with molecular orbital theory.<sup>27,28</sup> The energies of these two eigenmodes are determined by the strength of the interaction between the sphere and cavity plasmons, which is controlled by the thickness of the shell layer. A thin shell results in strong plasmon mixing, while a thick shell effectively isolates the plasmons of the two surfaces. The symmetric mode  $|\omega_-|$  is assigned when the inner and outer surfaces of the nanoshell are similarly polarized (large net dipole moment), while the

\* Corresponding author. E-mail: halas@rice.edu.

<sup>†</sup> Department of Chemistry.

<sup>‡</sup> Department of Electrical and Computer Engineering.

<sup>§</sup> Current Address: Air Force Research Laboratory, Wright-Patterson AFB, OH.

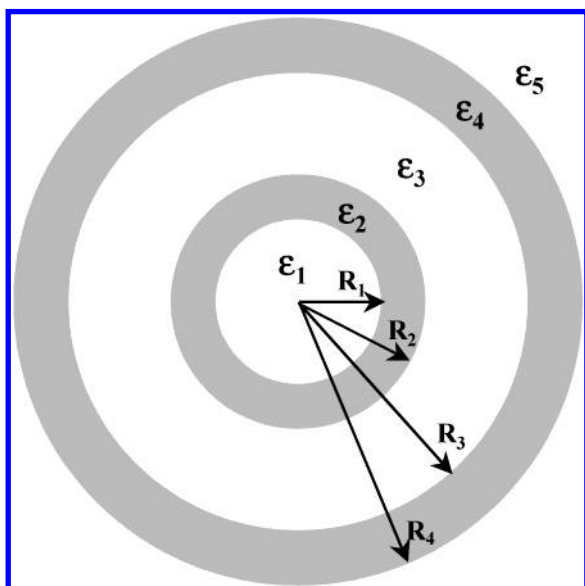


**Figure 1.** Schematic of a concentric nanoshell where  $\epsilon_1$ ,  $\epsilon_3$  are composed of  $\text{SiO}_2$ ,  $\epsilon_2$ ,  $\epsilon_4$  are composed of Au, and  $\epsilon_5$  is the embedding medium.

antisymmetric mode  $|\omega_+\rangle$  is assigned when the inner and outer surfaces are oppositely polarized. The antisymmetric “antibonding” plasmon mode is at higher energies than the symmetric “bonding” plasmon mode. This seemingly contradictory result is caused by the fact that the plasmons are incompressible deformations of the valence electrons of the metallic shell.<sup>29</sup>

In this paper we discuss the properties of a concentric nanoshell, a multilayer metallodielectric nanoparticle whose plasmonic response can be understood using the plasmon hybridization model. A concentric nanoshell consists of alternating layers of dielectric and metal, essentially a nanoshell enclosed within another nanoshell, inspiring its alternative name of “nanomatryushka”. The concentric nanoshell particle is constructed by first growing a uniform nanoscale layer of gold around a silica nanoparticle core,<sup>9</sup> then coating this nanoparticle with a silica layer of controlled thickness,<sup>30</sup> followed by a second thin layer of gold. A schematic depicting the composition of this particle is shown in Figure 1. By fabricating a four-layer concentric nanoshell particle, it is possible to independently tune the energies of the inner shell and outer shell plasmons, as well as the strength of the interaction between the inner and outer shell plasmons, thus controlling most aspects of the overall resonant response of the nanostructure.

The plasmon–plasmon interaction of the inner and outer metal shells in a concentric nanoshell results in a hybridization of the symmetric and antisymmetric nanoshell plasmon resonances (Figure 2). The energy level diagram in Figure 2a depicts the hybridization of the concentric nanoshell plasmons in terms of the mixing of the inner and outer shell plasmons. The experimentally observable eigenmodes of the concentric nanoshell plasmon resonance are indicated. The observable eigenmodes correspond to the hybridization of the symmetric modes of the two metal shell layers. In the case of the concentric nanoshell plasmon, the antisymmetric

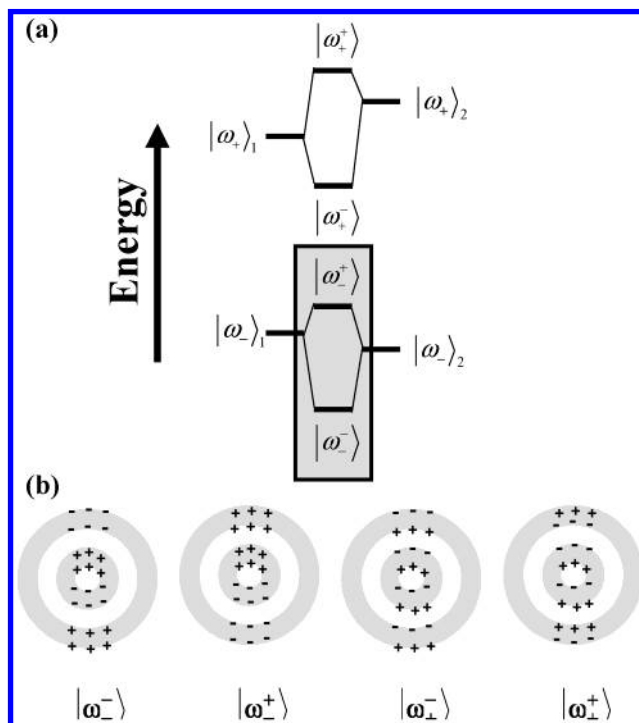


**Figure 2.** (a) Energy level diagram of the plasmon modes of a concentric nanoshell, depicted in terms of the “bonding” and “antibonding” modes of the inner and outer nanoshell of the composite nanostructure; (b) induced polarizations of the concentric nanoshell modes.

plasmon mode  $|\omega_-\rangle$  is of lower energy and has a smaller dipole moment than the symmetrically polarized hybrid plasmon  $|\omega_+\rangle$ . The induced dipole moments at the metallic interfaces of the concentric nanoshell plasmon modes are shown schematically in Figure 2b. The symmetrically polarized eigenmode  $|\omega_+\rangle$  has a higher energy due to the increased electrostatic repulsion at its internal adjacent interfaces occurring for this plasmon excitation. The relative energies of the hybrid modes are tuned by controlling the strength of the plasmon–plasmon interaction between the shell layers, which in the concentric nanoshell case is achieved by controlling the thickness of the dielectric layer  $R_3$  between the two metal shells.

The energies of the plasmon resonances for a nanoshell particle and also for a concentric nanoshell can be calculated using Mie scattering theory. The calculated optical extinction spectra are shown in Figure 3. The differences in dipole moments for the various plasmon modes directly influence how strongly the nanoparticle plasmon couples to the optical field, which is reflected in the magnitude of the extinction resonance for the various modes. For a single nanoshell plasmon, the higher energy  $|\omega_+\rangle$  symmetric mode couples only weakly to the optical field, resulting in a much weaker optical resonance (Figure 3a).<sup>27</sup> Using a Drude model for the dielectric function we predict this resonance to occur at approximately 8.2 eV, or at a wavelength of  $\sim 150$  nm in the vacuum ultraviolet region of the spectrum. Due to the weak optical polarizability of the  $|\omega_+\rangle$  mode, as well as its resonant energy, which for Au corresponds to a region of strong optical absorption due to interband effects, it is likely

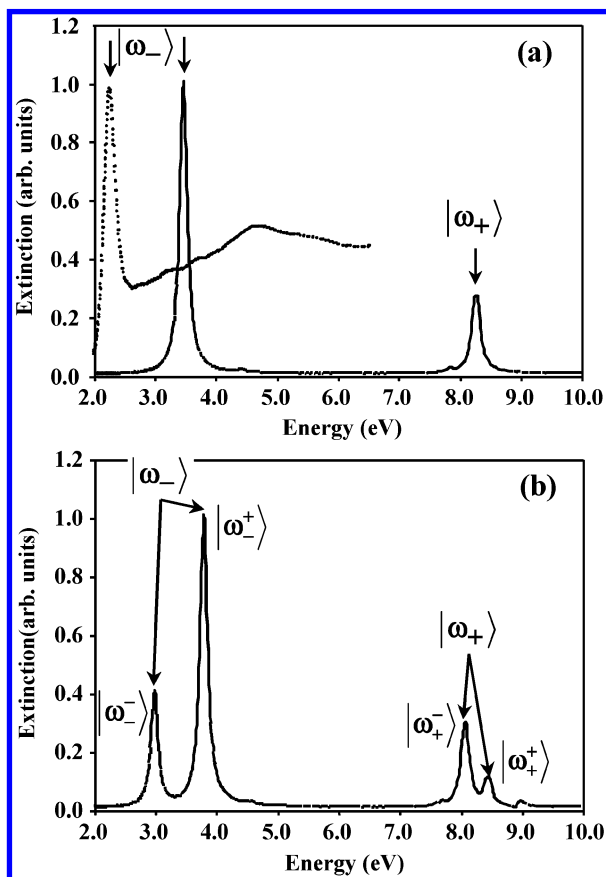


**Figure 3.** (a) Theoretical extinction spectrum for a nanoshell (SiO<sub>2</sub> core, Au shell) calculated using a Drude dielectric function (solid line) and an experimentally obtained dielectric function (dotted line) for Au (the experimental dielectric function does not extend to the energy range of the antisymmetric  $|\omega_+ \rangle$  eigenmode of the plasmon resonance). (b) The theoretical extinction spectrum for a concentric nanoshell particle calculated using a Drude dielectric function. In this geometry both the symmetric  $|\omega_- \rangle$  and antisymmetric  $|\omega_+ \rangle$  eigenmodes undergo plasmon hybridization. ( $R_1 = 9$  nm;  $R_2 = 12$  nm;  $R_3 = 17$  nm;  $R_4 = 22.67$ ;  $R_1/R_2 = R_3/R_4 = 0.75$ ).

that this mode would be quite difficult to observe using optical methods. The stronger  $|\omega_- \rangle$  resonance is calculated using both a Drude dielectric function as well as the empirically obtained dielectric values for Au, Figure 3a. For concentric nanoshells the Drude dielectric function predicts the four resonances arising from the plasmonic mixing discussed above, with the relative peak heights relating to the polarizabilities of the various plasmon modes, Figure 3b. From these calculations we can infer that, within our experimentally accessible UV–visible spectral range, mixing of the  $|\omega_- \rangle$  resonances of the inner and outer shells to form the hybridized resonances  $|\omega_-^- \rangle$  and  $|\omega_-^+ \rangle$  of the concentric nanoshell should be clearly observable.

Experimental synthesis of concentric nanoshells has been recently reported.<sup>25</sup> Silica nanoparticles were synthesized via the Stober method.<sup>31</sup> The nanoparticles were then derivatized with (aminopropyl)triethoxysilane (APTES) to attach small Au colloids (2–3 nm in diameter). The small colloidal nanoparticles attached to the silica nanoparticle surface served as nucleation sites for the electroless plating of a metallic film onto the nanoparticle surface. Once complete,

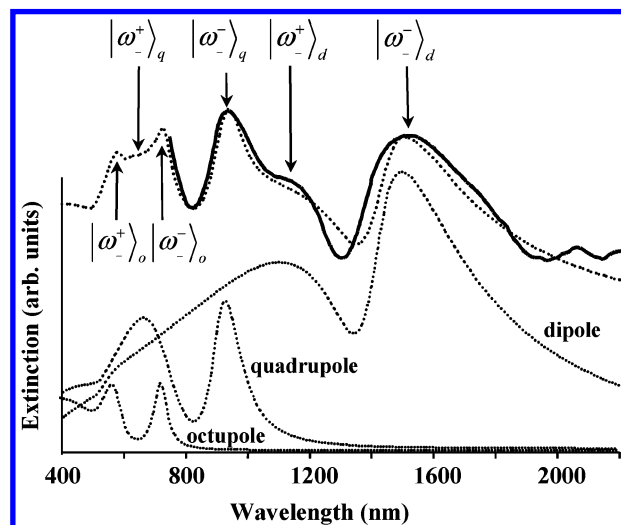


**Figure 4.** Experimentally measured extinction spectrum of a concentric nanoshell particle (solid line) and the theoretical extinction spectrum (dashed line) calculated using an experimentally obtained dielectric function for gold. The various order multipoles of the plasmon are plotted individually (dotted lines) to show the multimodal structure of the overall concentric nanoshell plasmon response. The modes are labeled on the total extinction spectrum.

this metallic shell layer supports optical resonances characteristic of the plasmon response of a silica–gold core–shell nanoparticle.<sup>9</sup> The gold surface was then functionalized with APTES preparing the nanoparticles for condensation of a uniform silica layer onto their surfaces using a dilute sodium silicate solution.<sup>30</sup> This thin silica layer was further increased using the chemistry of the Stober method on the already-grown nanoparticles. Once the silica layer reached the desired thickness, it was capped with a second Au layer prepared using the seeded-reduction chemistry used on the inner Au layer. Extinction spectra were obtained using a Nicolet FTIR instrument. Samples were prepared for spectral measurements by derivatizing the concentric nanoshells with 1-dodecanethiol and either dispersing in CS<sub>2</sub> solvent in a 1 mm path length cell, or by drying, mixing with KBr, and pressing the sample into pellet form.

By analyzing the extinction spectrum of concentric nanoshells we can elucidate peak assignments and structural features unambiguously and investigate the onset of phase retardation (or finite size) effects in nanostructures of experimentally realizable dimensions. The experimental extinction spectrum of concentric nanoshells is shown in Figure 4. This spectrum was obtained for SiO<sub>2</sub>/Au/SiO<sub>2</sub>/Au nanoshells of dimensions  $R_1/R_2/R_3/R_4 = 80/107/135/157$  nm, respectively. In this spectrum the observed resonances are due to the strong mixing of the  $|\omega_- \rangle$  modes of the inner shell and of the outer shell. The hybridized resonances  $|\omega_-^- \rangle$  and  $|\omega_-^+ \rangle$  are noted. Due to the size of the composite nanoparticle, higher order multipole modes are excited in the shell layers and participate in the plasmon hybridization. The multipole contributions from each shell layer mix with each other and contribute to the overall plasmon response of the nanostructure. In this case the quadrupole and octupole hybrid plasmon modes are responsible for the higher energy resonant response measured in this structure.

In the small nanoparticle (quasistatic) limit the energy splitting due to plasmon hybridization in a concentric nanoshell is expected to be relatively symmetric in energy, in direct analogy with molecular orbital theory.<sup>25</sup> The interaction between the  $|\omega_{-}\rangle$  and the  $|\omega_{+}\rangle$  plasmons on different shells within the nanostructure is very weak and does not induce a visible asymmetry. For finite sized particles, however, the observed plasmon splitting is strongly asymmetric, with all states shifted to lower energies. We have investigated this size dependence theoretically, by studying the nanoparticle size dependence of the splitting asymmetry. We examine the onset of this asymmetric splitting for two dielectric functions: a Drude model, which neglects the contributions of the d-band electrons to the dielectric function of the metal, and an empirical dielectric function.<sup>32</sup> These calculations use the same approach described previously for the single-layer nanoshell and neglect contributions due to electron scattering that lead to homogeneous broadening of the resonances. The results of these calculations are presented in Figure 5, which shows the absolute difference in hybrid peak position of  $|\omega_{-}^{-}\rangle$  and  $|\omega_{-}^{+}\rangle$  with respect to the single-layer, inner nanoshell plasmon eigenmode  $|\omega_{-}\rangle$  as a function of total particle size. The particle size was determined by holding the core-to-shell ratio,  $R_c/R_s$ , constant for both the inner and outer metal shells, which ensures that the single-layer plasmon resonance for each shell is at the same frequency. The total particle size was increased by approximately 2–5% to generate each data point. In both Figure 5a and 5b, the hybrid modes are split symmetrically for small nanoparticle size, as evidenced by the overlay of the symmetric  $|\omega_{-}^{+}\rangle$  and antisymmetric  $|\omega_{-}^{-}\rangle$  modes in each graph (region (i)). As particle size increases, an anisotropic red shift in the peak plasmon positions is seen as both plasmon resonances shift to lower energies, with the shifts being stronger for the lower energy eigenmodes (region (ii)). With increasing nanoparticle size the position of the higher energy mode is eventually red shifted with respect to the nonhybridized inner nanoshell plasmon (region (iii)).

This anisotropy in the plasmon splitting appears to be related to finite size, or phase retardation, as the nanoparticle dimensions become larger with respect to the spatial wavelength of light at the plasmon resonance. The onset of higher order multipolar resonances strongly influences the position of the hybrid peak positions of the dipole resonance. This explains the two trends that are seen in Figure 5: the higher energy plasmon mode (shorter plasmon resonant wavelength) begins to red-shift at lower nanoparticle sizes and shifts more strongly than the lower energy plasmon mode (longer plasmon resonant wavelength). This trend is seen for both of the dielectric functions used in the calculations. The difference between the two dielectric functions, namely the inclusion of the d electrons, shifts the plasmon resonance to longer wavelengths, as seen in the spectra in Figure 3a. This is seen in the comparison between Figure 5a and 5b as well, where the size dependence of the asymmetry is markedly less strong for the empirical dielectric function where the plasmon resonances occur at longer wavelengths than for the Drude case.

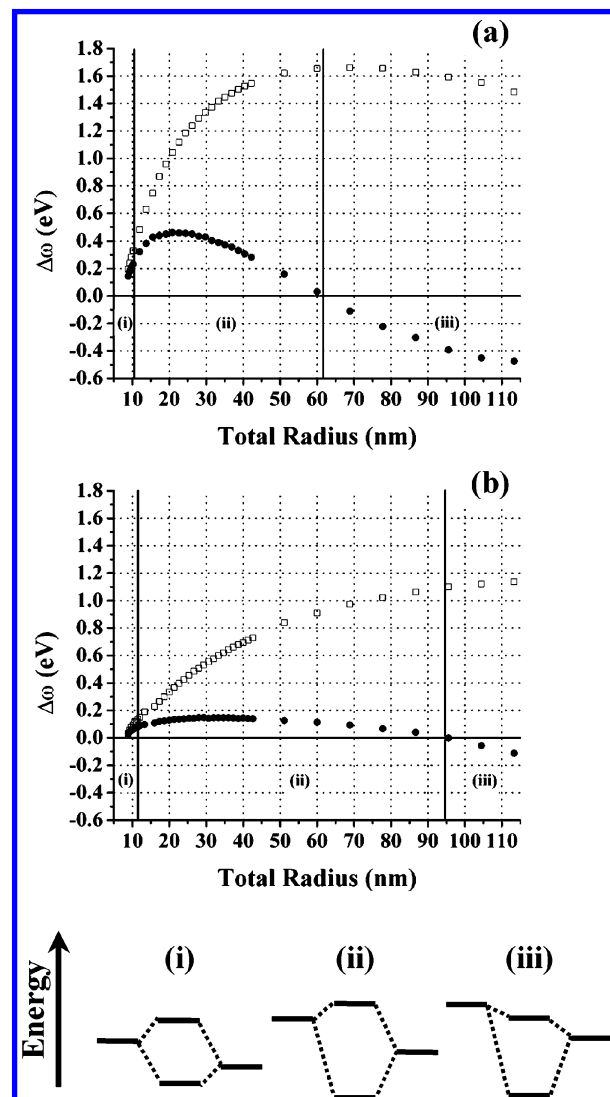


**Figure 5.** Theoretical calculations showing the effects of finite size on the splitting asymmetry of the concentric nanoshell eigenmodes. (a) Calculations performed with a modified Drude dielectric function. (b) Calculations using the experimentally obtained dielectric function (Au). The diagram denotes the onset of asymmetry in the hybrid plasmon splitting: (i) at small particle sizes the hybrid plasmon modes split symmetrically; (ii) beyond the quasistatic limit the hybrid modes split anisotropically, with the higher energy mode redshifting more strongly than the lower energy mode; (iii) at larger nanoparticle sizes both modes are red shifted, the higher energy eigenmode shifts to lower energies than the (unhybridized) inner nanoshell plasmon energy ( $R_1/R_2 = R_3/R_4 = 0.75$  in all calculations).

In this work we have examined the role plasmon hybridization in the concentric nanoshell plasmonic nanostructure. The complex structure of the concentric nanoshell plasmon was shown to be a sum of the contributions of the dipolar and higher order hybrid multipolar plasmon modes. Finite size effects appear to induce a strong red shift in the energies of the hybridized plasmon modes of the concentric nanoshell with respect to the single-layer nanoshell plasmon mode  $|\omega_{-}\rangle$ . This red shift appears to be characteristic of finite size, or phase retardation, effects. Excellent agreement between Mie scattering theory and the experimentally measured plasmon



response of the nanostructure allows for a detailed interpretation of the interaction between these plasmon modes.

**Acknowledgment.** The authors thank the Army Research Office, the Air Force Office of Scientific Research, the National Science Foundation, the Robert A. Welch Foundation, and NASA for support of this work.

## References

- (1) Aizpurua, J.; Hanarp, P.; Sutherland, D. S.; Kall, M.; Bryant, G. W.; Garcia de Abajo, F. J. *Phys. Rev. Lett.* **2003**, *90*, 057401.
- (2) Haynes, C. L.; Van Duyne, R. P. *J. Phys. Chem. B* **2003**, *107*, 7426.
- (3) Jackson, J. B.; Westcott, S. L.; Hirsch, L. R.; West, J. L.; Halas, N. J. *Appl. Phys. Lett.* **2003**, *82*, 257.
- (4) Haes, A. J.; Van Duyne, R. P. *J. Am. Chem. Soc.* **2002**, *124*, 10596.
- (5) Sershen, S. R.; Westcott, S. L.; Halas, N. J.; West, J. L. *J. Biomed. Mater. Res.* **2000**, *51*, 293.
- (6) Maier, S. A.; Brongersma, M. L.; Kik, P. G.; Atwater, H. A. *Phys. Rev. B* **2002**, *65*, 193408.
- (7) Nikoobakht, B.; El-Sayed, M. A. *Chem. Mater.* **2003**, *15*, 1957.
- (8) Nicewarner-Pena, S. R.; Griffith-Freeman, R.; Reiss, B. D.; He, L.; Pena, D. J.; Walton, I. D.; Cromer, R.; Keating, C. D.; Natan, M. J. *Science* **2001**, *294*, 137.
- (9) Oldenburg, S. J.; Averitt, R. D.; Westcott, S.; Halas, N. J. *Chem. Phys. Lett.* **1998**, *288*, 243.
- (10) Graf, C.; van Blaaderen, A. *Langmuir* **2002**, *18*, 524.
- (11) Love, J. C.; Gates, B. D.; Wolfe, D. B.; Paul, K. E.; Whitesides, G. M. *Nano Lett.* **2002**, *2*, 891.
- (12) Charnay, C.; Lee, A.; Man, S.-Q.; Moran, C. E.; Radloff, C.; Bradley, R. K.; Halas, N. J. *J. Phys. Chem. B* **2003**, *107*, 7327.
- (13) Aguirre, C.; Kaspar, T.; Radloff, C.; Halas, N. J. *Nano Lett.* **2003**, *3*, 1707.
- (14) Xia, Y.; Whitesides, G. M. *Angew. Chem., Intl. Ed.* **1998**, *37*, 550.
- (15) Moran, C. E.; Radloff, C.; Halas, N. J. *Adv. Mater.* **2003**, *15*, 804.
- (16) Sun, Y.; Xia, Y. *Anal. Chem.* **2002**, *74*, 5297.
- (17) Kneipp, K.; Kneipp, H.; Itzkan, I.; Dasari, R. R.; Feld, M. S. *Chem. Rev.* **1999**, *99*, 2957.
- (18) Maier, S. A.; Brongersma, M. L.; Kik, P. G.; Meltzer, S.; Requicha, A. A. G.; Atwater, H. A. *Adv. Mater.* **2001**, *13*, 1501.
- (19) Mie, G. *Ann. Phys.* **1908**, *25*, 377.
- (20) Aden, A. L.; Kerker, M. *J. Appl. Phys.* **1951**, *22*, 1242.
- (21) Sinzig, J.; Quinten, M. *Appl. Phys. A* **1994**, *58*, 157.
- (22) Sarkar, D.; Halas, N. J. *Phys. Rev. E* **1997**, *56*, 1102.
- (23) Kelly, K. L.; Eduardo, C.; Zhao, L. L.; Schatz, G. C. *J. Phys. Chem. B* **2003**, *107*, 668.
- (24) Jensen, T.; Kelly, L.; Lazarides, A.; Schatz, G. C. *J. Cluster Sci.* **1999**, *10*, 295.
- (25) Prodan, E.; Radloff, C.; Halas, N. J.; Nordlander, P. *Science* **2003**, *302*, 419.
- (26) Prodan, E.; Nordlander, P.; Halas, N. J. *Nano Lett.* **2003**, *3*, 1411.
- (27) Prodan, E.; Nordlander, P. *Chem. Phys. Lett.* **2002**, *352*, 140.
- (28) Prodan, E.; Nordlander, P. *Nano Lett.* **2003**, *3*, 543.
- (29) Prodan, E.; Nordlander, P. *J. Chem. Phys.* **2004**, *120*, 5444.
- (30) Liz-Marzan, L. M.; Giersig, M.; Mulvaney, P. *Langmuir* **1996**, *12*, 4329.
- (31) Stober, W.; Fink, A.; Bohn, E. *J. Colloid Interface Sci.* **1968**, *26*, 62.
- (32) Johnson, P. B.; Christy, R. W. *Phys. Rev. B* **1972**, *6*, 4370.

NL049597X